

# Effects of Al<sub>2</sub>O<sub>3</sub> on the piezoelectric properties of Pb(Mn<sub>1/3</sub>Nb<sub>2/3</sub>)O<sub>3</sub>-PbZrO<sub>3</sub>-PbTiO<sub>3</sub> ceramics

Young-Min Kim · Jae-Chang Kim · Soon-Chul Ur · Il-Ho Kim

© Springer Science + Business Media, LLC 2006

**Abstract** Piezoelectric properties of Al<sub>2</sub>O<sub>3</sub>-doped Pb(Mn<sub>1/3</sub>Nb<sub>2/3</sub>)O<sub>3</sub>-PbZrO<sub>3</sub>-PbTiO<sub>3</sub> ceramics were investigated. The constituent phases, microstructure, electromechanical coupling factor, dielectric constant, piezoelectric charge and voltage constants were analyzed. Diffraction peaks for (002) and (200) planes were identified by X-ray diffractometer for all the specimens doped with Al<sub>2</sub>O<sub>3</sub>. The highest sintered density of 7.8 g/cm<sup>3</sup> was obtained for 0.2 wt% Al<sub>2</sub>O<sub>3</sub>-doped specimen. Grain size increased by doping Al<sub>2</sub>O<sub>3</sub> up to 0.3 wt%, and it decreased by more doping. Electromechanical coupling factor, dielectric constant, piezoelectric charge and voltage constants increased by doping Al<sub>2</sub>O<sub>3</sub> up to 0.2 wt%, and it decreased by more doping. This might result from the formation of oxygen vacancies due to defects in O<sup>2-</sup> ion sites and the substitution of Al<sup>3+</sup> ions.

**Keywords** PZT · Piezoelectric · Al<sub>2</sub>O<sub>3</sub> doping

## 1 Introduction

Piezoelectric ceramics are widely used for ultrasonic devices, ignition devices, piezoelectric buzzers, actuators, oscillators, and RF filters. Since the piezoelectric phenomenon has

been discovered in BaTiO<sub>3</sub> by applying high DC bias [1], many researches on piezoelectrics have been progressed. Pb(Zr,Ti)O<sub>3</sub> (PZT), solid solution of PbZrO<sub>3</sub> and PbTiO<sub>3</sub>, has been developed by B. Jaffe [2]. However, plenty of problems and obstacles are remained, such as weak mechanical strength, strong dependence of dielectric property on frequency, high dielectric loss below maximum operating temperature, use in volatile and toxic PbO, difficulty in preparing pure perovskite phases not involving pyrochlore phases [3, 4].

Since the pure PZT is difficult to perform sintering and polarization, and its electrical properties are unstable, generally additives such as MnO<sub>2</sub> and Al<sub>2</sub>O<sub>3</sub> are employed. Complex perovskites have been studied by substituting B-sites (Zr or Ti sites) of perovskite structure with 2<sup>+</sup>, 3<sup>+</sup>, 5<sup>+</sup> or 6<sup>+</sup> metal ions [5, 6]. These additives or dopants make complete solid solution with tetragonal PbTiO<sub>3</sub> and orthorhombic PbZrO<sub>3</sub>, and produce antiferroelectrics or ferroelectrics with MPB (morphotropic phase boundary) compositions showing maximum variations of dielectric, piezoelectric properties and electromechanical coupling factor. In addition, perovskite structure can be maintained by the additives not lowering the Curie temperature. In this study, Pb(Mn<sub>1/3</sub>Nb<sub>2/3</sub>)O<sub>3</sub>-PbZrO<sub>3</sub>-PbTiO<sub>3</sub>-based ceramics were prepared and their piezoelectric properties were investigated with Al<sub>2</sub>O<sub>3</sub> content.

## 2 Experimental procedure

0.05Pb(Mn<sub>1/3</sub>Nb<sub>2/3</sub>)O<sub>3</sub>-0.45PbZrO<sub>3</sub>-0.50PbTiO<sub>3</sub> (shortly, PMN-PZT) was prepared by mixing and milling PbO, MnO<sub>2</sub>, Nb<sub>2</sub>O<sub>5</sub>, ZrO<sub>2</sub> and TiO<sub>2</sub> powders. Al<sub>2</sub>O<sub>3</sub> was added to increase sintered density and to lower sintering temperature, and 2.0 wt% excess PbO was used to compensate its volatilization

Y.-M. Kim · J.-C. Kim  
Department of Materials Development, Corea Electronics Corporation (CEC), 168-16 Yongtan-dong, Chungju, Chungbuk 380-250, Korea

S.-C. Ur · I.-H. Kim (✉)  
Department of Materials Science and Engineering/ReSEM, Chungju National University, 123 Geomdan-ri, Iryu-myeon, Chungju, Chungbuk 380-702, Korea  
e-mail: ihkim@chungju.ac.kr

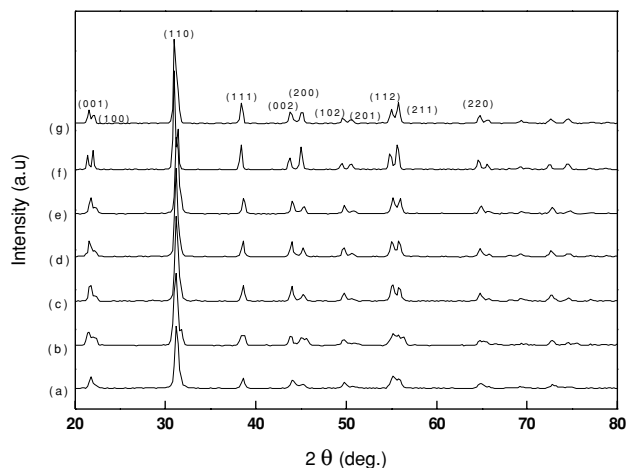


**Fig. 1** X-ray diffraction patterns of  $\text{Al}_2\text{O}_3$ -doped PMN-PZT ceramics sintered at  $1100^\circ\text{C}$  for 1 h: (a) 0.0 wt%, (b) 0.1 wt%, (c) 0.2 wt%, (d) 0.3 wt%, (e) 0.4 wt%, (f) 0.5 wt%, and (g) 1.0 wt%

during the high temperature sintering. Mixed powders were ball-milled with zirconia balls and ethyl alcohol in a polyurethane vessel for 24 h, and then dried and calcined at  $900^\circ\text{C}$  for 2 h in an alumina crucible to synthesize precursors. Calcined powders were ground in an alumina mortar and ball-milled for 24 h again. 1.0 wt% PVA (poly vinyl alcohol) was added before finishing milling to make slurry and it was dried by the spray dryer. The dried powders were sieved under #140 mesh and compacted to disc-type ( $31.7 \phi \times 3.1 \text{ mm}$ ) specimens at a pressure of  $1000 \text{ kgf/cm}^2$ . The compacts were sintered at  $1100^\circ\text{C}$  to  $1200^\circ\text{C}$  for 1 h.

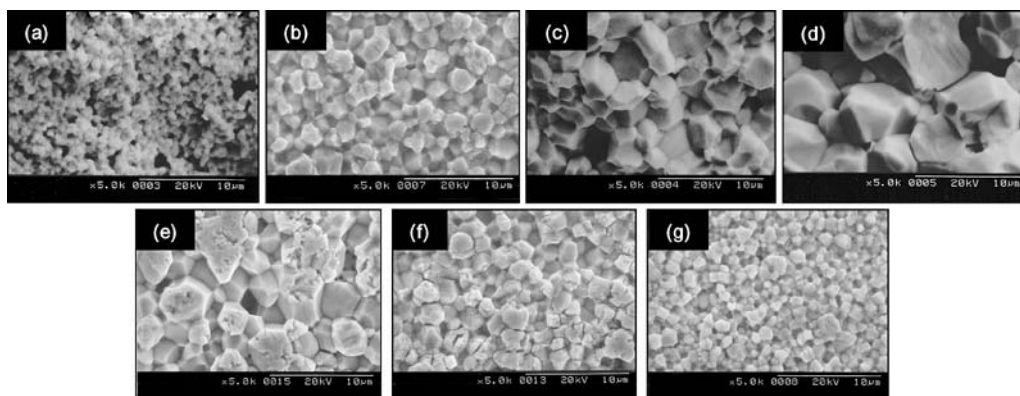
Sintered density was measured by the ASTM C373-72 method, and the constituent phases of the calcined and sintered samples were analyzed by the X-ray diffractometer (XRD). In order to observe microstructures by the scanning electron microscope (SEM), fractured surfaces of sintered pellets were polished and chemically etched with  $\text{HF:HCl:H}_2\text{O} = 0.5:5:94.5$  solution for 10 s. Silver conductive paste (#3288, Metech Inc.) was coated to both sides of sintered specimens and heated at  $600^\circ\text{C}$  for

20 min to make electrodes for measuring dielectric and piezoelectric properties. Poling was carried out in a silicon oil bath by applying  $3 \text{ kV/mm}$  of electric field for 20 min, and aging treatment was performed for 24 h to release internal stresses. Relative dielectric constant ( $\epsilon$ ), electromechanical coupling factor ( $k_p$ ) and mechanical quality factor ( $Q_m$ ) were analyzed by measuring resonance frequency ( $f_r$ ), antiresonance frequency ( $f_a$ ) and resonance resistance ( $R$ ) through the IRE Standards [7].

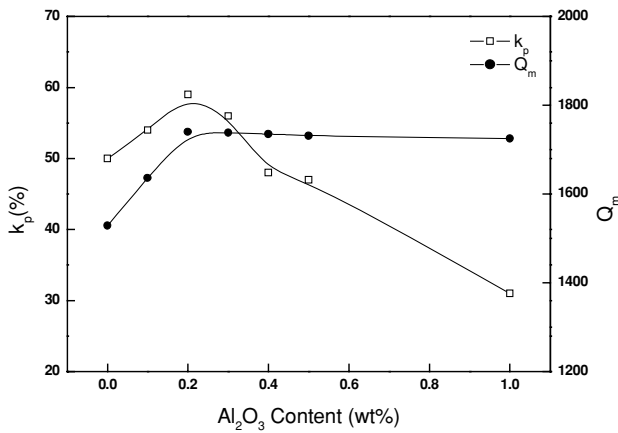
### 3 Results and discussion

Figure 1 shows the XRD patterns of  $\text{Al}_2\text{O}_3$ -doped PMN-PZT ceramics sintered at  $1100^\circ\text{C}$  for 1 h. For all the specimens diffraction peaks for (002) and (200) planes in the range of diffraction angle,  $2\theta = 42\text{--}46^\circ$  were identified, which means the tetragonal or coexistence of rhombohedral and tetragonal structure. Slight shift in diffraction angle by doping  $\text{Al}^{3+}$  ions indicates their substitution (solid solution) into the lattice of PZT.  $\text{Al}^{3+}$  ions are expected to substitute B-sites of the perovskite structure, because ionic radius of  $\text{Al}^{3+}$  ( $0.57 \text{ \AA}$ ) is more similar to that of  $\text{Zr}^{4+}$  ( $0.79 \text{ \AA}$ ) or  $\text{Ti}^{4+}$  ( $0.68 \text{ \AA}$ ) than that of  $\text{Pb}^{2+}$  ( $1.32 \text{ \AA}$ ). There are no specific changes in diffraction peaks with sintering temperature up to  $1200^\circ\text{C}$ .

Density variations of specimens sintered at  $1100^\circ\text{C}$  for 1 h with  $\text{Al}_2\text{O}_3$  content were investigated. Sintered density of  $6.9 \text{ g/cm}^3$  for undoped specimen showed peak value of  $7.8 \text{ g/cm}^3$  for 0.2 wt%  $\text{Al}_2\text{O}_3$ -doped specimen, expecting promotion of sintering by eutectic reaction of  $\text{Al}_2\text{O}_3$  and  $\text{PbO}$ . Figure 2 shows the microstructural variation with  $\text{Al}_2\text{O}_3$  content when sintered at  $1100^\circ\text{C}$  for 1 h. Grain size increased with increasing  $\text{Al}_2\text{O}_3$  content up to 0.3 wt%, and decreased by more doping. This might result from the increase in lattice constants and lattice volumes due to substitutions of  $\text{Al}^{3+}$  ions up to 0.3 wt%  $\text{Al}_2\text{O}_3$  addition, and from the suppression



**Fig. 2** SEM photographs of  $\text{Al}_2\text{O}_3$ -doped PMN-PZT ceramics sintered at  $1100^\circ\text{C}$  for 1 h: (a) 0.0 wt%, (b) 0.1 wt%, (c) 0.2 wt%, (d) 0.3 wt%, (e) 0.4 wt%, (f) 0.5 wt%, and (g) 1.0 wt%



**Fig. 3** Variation of electromechanical coupling factor ( $k_p$ ) and mechanical quality factor ( $Q_m$ ) with  $\text{Al}_2\text{O}_3$  content in PMN-PZT ceramics

of grain growth due to existence of unsubstituted  $\text{Al}^{3+}$  ions at grain boundaries by more  $\text{Al}_2\text{O}_3$  addition. Similar result was reported [8] for the ZnO-doped  $0.05\text{Pb}(\text{Mn}_{1/3}\text{Nb}_{2/3})\text{O}_3$ - $0.45\text{PbZrO}_3$ - $0.50\text{PbTiO}_3$  ceramics. R.B. Atkim et al. [9] have analyzed that dopant ions are concentrated at grain boundaries and they take excess impurities by diffusion when grain boundaries move, which reduces grain boundary mobility and size.

Figure 3 represents the variation of electromechanical coupling factor ( $k_p$ ) and mechanical quality factor ( $Q_m$ ) with  $\text{Al}_2\text{O}_3$  content. Maximum  $k_p$  of 60% was obtained when 0.2 wt%  $\text{Al}_2\text{O}_3$  was doped, and  $Q_m$  was saturated to around 1780 when  $\text{Al}_2\text{O}_3$  was doped over than 0.2 wt%. This was related with solid solution limit of  $\text{Al}^{3+}$  ions and microstructural variation. F. Kulcsar et al. [10] have reported that in the case of substitution of  $3^+$  ions for B-sites of the perovskite structure, oxygen vacancies produced by charge neutrality beyond solid solution limit lead to decrease in electromechanical coupling factor, dielectric constant and electrical resistivity, and

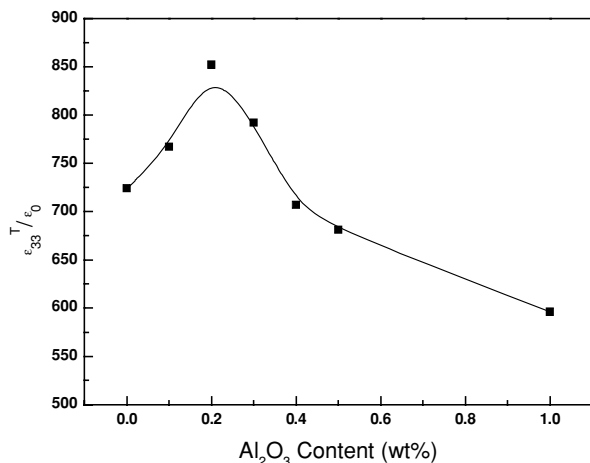


**Fig. 4** Variation of relative dielectric constant ( $\epsilon_{33}^T/\epsilon_0$ ) with  $\text{Al}_2\text{O}_3$  content in PMN-PZT ceramics

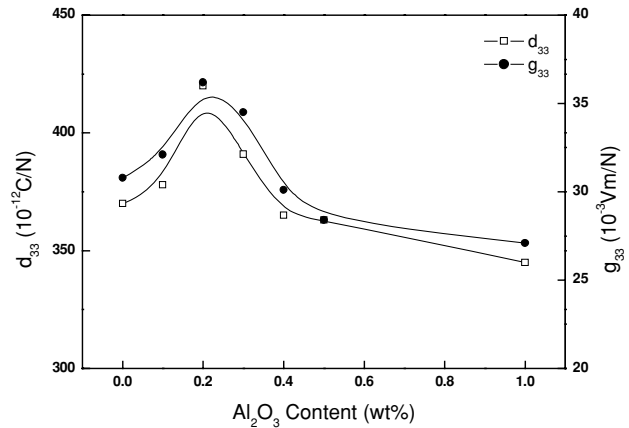


**Fig. 5** Variation of piezoelectric charge constant ( $d_{33}$ ) and voltage constant ( $g_{33}$ ) with  $\text{Al}_2\text{O}_3$  content in PMN-PZT ceramics

to increase in mechanical quality factor and coercive force. Figure 4 indicates the variation of relative dielectric constant ( $\epsilon_{33}^T/\epsilon_0$ ) with  $\text{Al}_2\text{O}_3$  content. Maximum value was obtained for 0.2 wt%  $\text{Al}_2\text{O}_3$ -doped specimen, resulting from the reason mentioned before.

Figure 5 shows the variation of piezoelectric charge constant ( $d_{33}$ ) and voltage constant ( $g_{33}$ ) with  $\text{Al}_2\text{O}_3$  content. As expected, both  $d_{33}$  and  $g_{33}$  reached the maximum values when 0.2 wt%  $\text{Al}_2\text{O}_3$  was doped. In general, atoms substituting A-sites of the perovskite structure change the a-axis length of the lattice, and atoms substituting B-sites change the c-axis length. Therefore, c/a axis ratio (tetragonality) is changed by doping. Dielectric and piezoelectric properties can be enhanced due to the increase in dipole moment of the unit cell by increasing c/a axis ratio.  $\text{Al}^{3+}$  ions have possibility to substitute B-sites, and improvements in dielectric and piezoelectric properties are expected when  $\text{Al}_2\text{O}_3$  is doped up to solid solution limit, which is estimated to 0.2–0.3 wt% for the PMN-PZT system.

#### 4 Conclusions

Dielectric and piezoelectric properties and microstructures of  $\text{Pb}(\text{Mn}_{1/3}\text{Nb}_{2/3})\text{O}_3$ - $\text{PbZrO}_3$ - $\text{PbTiO}_3$  ceramics were investigated with the amount of  $\text{Al}_2\text{O}_3$  additive. X-ray diffraction peaks for (002) and (200) planes of all the specimens doped with  $\text{Al}_2\text{O}_3$  revealed the tetragonal or coexistence of rhombohedral and tetragonal structure. Density was remarkably increased when sintered at  $1100^\circ\text{C}$ , and the highest sintered density of  $7.8 \text{ g/cm}^3$  was obtained for the 0.2 wt%  $\text{Al}_2\text{O}_3$ -doped specimen. Grain size increased by doping  $\text{Al}_2\text{O}_3$  up to 0.3 wt% and decreased by more doping. It was considered that partly unsubstituted  $\text{Al}^{3+}$  ions existed at grain boundaries and suppressed the grain growth. Dielectric and piezoelectric properties reached the maximum for the 0.2 wt%  $\text{Al}_2\text{O}_3$ -doped specimen. This might result from the solid

solution limit of  $\text{Al}^{3+}$  in the PMN-PZT system is around 0.2–0.3 wt%, and formation of oxygen vacancies in  $\text{O}^{2-}$  ion sites by charge neutrality beyond solid solution limit.

**Acknowledgments** This research was supported by the Program for the Training of Graduate Students in Regional Strategic Industries and the Regional Innovation Center (RIC) Program which were conducted by the Ministry of Commerce, Industry and Energy of the Korean Government.

## References

1. S. Robert, *Phys. Rev.*, **71**, 890 (1947).
2. B. Jaffe, R.S. Roth, and S. Marzullo, *J. Appl. Phys.*, **25**(26), 809 (1954).
3. R.F. Zhang, J. Ma, L.B. Kong, Y.Z. Chen, and T. S. Zhang, *Mater. Lett.*, **55**(6), 388 (2002).
4. Z. Brankavi, G. Brankovic, C. Jovalekic, Y. Maniette, M. Cilense, and J.A. Varela, *Mater. Sci. Eng., A*, **345**(1–2), 243 (2003).
5. S.Y. Chu, T.Y. Chen, and I.T. Tsai, *Mater. Lett.*, **58**(5), 752 (2004).
6. W.L. Zhang, Y.G. Wang, S.B. Yue, and P.L. Zhang, *Solid State Comm.*, **90**(6), 383 (1994).
7. IRE Standards, *Proc. IRE*, **49**, 1161 (1961).
8. Y.J. Son, D.Y. Hwang, J.C. Kim, K.W. Cho, Y.M. Kim, S.C. Ur, and I.H. Kim, *Kor. J. Mater. Res.*, **14**(11), 764 (2004).
9. R.B. Atkim and R.M. Fulrath, *J. Am. Ceram. Soc.*, **54**(5), 265 (1971).
10. F. Kulcsar, *J. Am. Ceram. Soc.*, **42**(7), 343 (1959).